The 9th European Congress on Computational Methods in Applied Sciences and Engineering
ECCOMAS Congress 2024
3 – 7 June 2024, Lisboa, Portugal

AERODYNAMIC INVESTIGATION OF A PROPELLER-DRIVEN TRANSPORT AIRCRAFT WITH DISTRIBUTED PROPULSION WITHIN THE IMOTHEP PROJECT

D. KELLER[1], A. VISINGARDI[2], L. WIART[3], Y. MALDONADO[4], AND F. MORLANDO[5]

[1] German Aerospace Center (DLR), Lilienthalplatz 7, 38108 Braunschweig, Germany
email: dennis.keller@dlr.de
[2] Centro Italiano Ricerche Aerospaziali (CIRA), Via Maiorise, 81043 Capua (CE), Italy
email: A.visingardi@cira.it
[3] Safran Tech, Rue des jeunes bois,78772 Magny-les-Hameaux, France
email: ludovic.wiart@safrangroup.com
[4] Safran Tech, Rue des jeunes bois, 78772 Magny-les-Hameaux, France
email: ye-bonne.maldonado@safrangroup.com
[5] Centro Italiano Ricerche Aerospaziali (CIRA), Via Maiorise, 81043 Capua (CE), Italy
email: fabrizio.morlando@cira.it

Key words: Aerodynamics, Propellers, Distributed (Hybrid-) Electric Propulsion.

Summary. The present publication illustrates the comprehensive collaborative work of Safran Tech, CIRA, and DLR that was carried out within the IMOTHEP project with regard to aero-propulsive aspects of a novel regional propeller-driven transport aircraft concept with distributed propulsion. Various numerical studies on basic aspects like propeller position as well as detailed design studies on propellers, propulsion integration, and high-lift devices were carried out. Different numerical methods ranging from unsteady vortex-lattice and surface vorticity panel methods to Reynolds-averaged Navier-Stokes computations were thereby utilized and compared with each other. The studies led to important design parameter sensitivities and recommendations that were subsequently fed back to the overall aircraft design. Moreover, the design studies yielded an increase of 10% in aerodynamic performance (L/D) compared to the initial design. Considering the slipstream effect during the high-lift design indicated a potential for improved climb performance.

1 INTRODUCTION

The demand for substantial CO_2 emission reductions in air traffic has led to an increasing research interest in air transport vehicles with (hybrid-) electric propulsion systems. While this type of propulsion system may introduce additional complexity and challenges, its usage also opens up the design space of aircraft configurations, in particular with respect to engine integration. A promising approach to benefit from this circumstance is to distribute the propulsion (DP) along the entire wing span. Besides potential positive effects on vertical tail plane size and aircraft weight due to flight mechanics and safety considerations [1], DP may also provide efficiency increases from an aerodynamic standpoint. Beneficial effects are thereby anticipated to originate from two sources with the first one being direct aero-propulsive efficiency increases during cruise flight and the second one being indirect benefits due to

improved high-lift capabilities. In cruise flight, the flexibility of DP systems may allow for aircraft performance increases due to improved propulsor integration. Configurational aspects with regard to aero-propulsive efficiency of DP were recently investigated by Keller [2] and Schollenberger et al. [3]. Besides these direct effects, DP systems promise increased high-lift capabilities in low speed, which in turn may yield benefits in cruise flight from wing sizing effects. With the light general aviation aircraft concept SCEPTOR, NASA tries to take advantage of this effect by utilizing high-lift propellers [4]. Keller [5] found an increase in lift generation of up to 42% for a regional aircraft configuration. Beckers et al. [6], Lindner et al. [7], Gothow et al. [8], Stoica et al. [9], and Visingardi et al. [10] carried out parametric studies on propeller-wing interaction of distributed propulsion systems on a wing section.

In the frame of the European IMOTHEP project the concept of a plug-in hybrid electric regional aircraft featuring distributed electric propulsion is investigated. As part of the assessment, extensive work has been carried out on the aerodynamics of the concept aircraft. The present paper gives an overview on this work. It first compares the various numerical methods used in the computation with regard to the estimation of the performance of an isolated propeller and propeller wing interaction. Moreover, selected results of several design studies on the effect of the propeller wing distance, nacelle integration, and high-lift capabilities are presented. Finally, results of a performance assessment are shown.

2 GEOMETRY

2.1 Basic Aircraft Design

The basis of the present investigation is the conceptual design of a regional transport aircraft carried out in the IMOTHEP Project [11]. The aircraft is designed for 40 passengers and a design mission range of 600 nm at a cruise Mach number of M_{cr}=0.4. The present aerodynamic studies are based on three different design loop stages (Figure 1), whose basic aircraft parameters are summarized in Table 1. A propeller design was carried out within the project for the initial aircraft design and updated along with the evolution of the airframe [12]. The propellers are all chosen to be identical along each wing side and are all rotating in inboard-up direction.

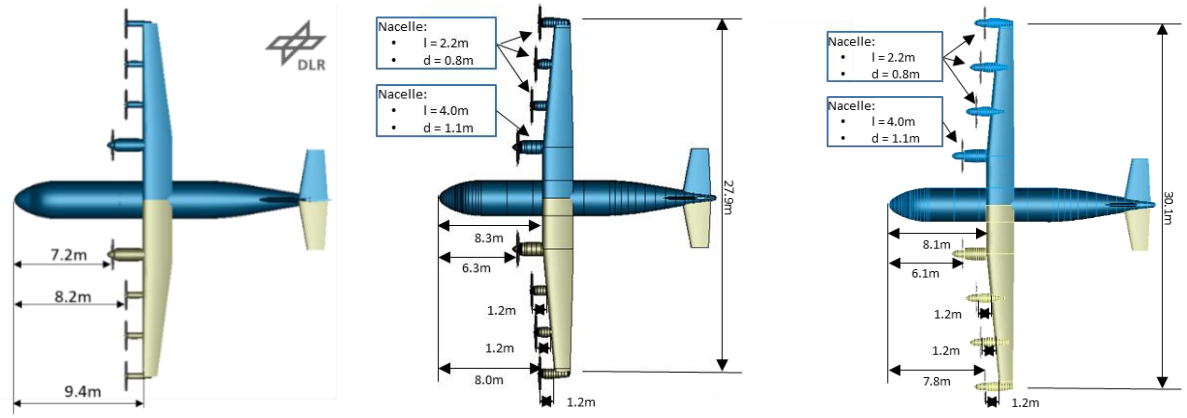

a) Loop 0 b) Loop 1 c) Loop 1.5

Figure 1: Conceptual aircraft design at various design stages

Table 1: Basic aircraft parameters of loop 0, loop 1, and loop 1.5 configurations

	Loop 0	Loop 1	Loop 1.5
Reference area	48.6 m^2	55.7 m^2	56.6 m^2
Half span	13.05 m	13.96 m	15.04 m
Aspect ratio	14	14	16
Sweep angle (l.e.)	0°	0° / 5.5°	0° / 5.5°
Mean aerodynamic chord	1.94 m	2.08 m	1.96 m
Propeller diameter	2.6 m	3.0 m	3.3 m

2.2 High Lift Design

A detailed aerodynamic high-lift design has been carried out for the loop 0 configuration by means of 2D-RANS optimizations for representative wing sections of the inboard and outboard flap. Propeller effects have not been considered during the optimizations. The resulting high-lift system features a single slotted dropped hinge flap with a relative flap chord length of 30% of the local chord and no leading-edge device. The high-lift design was later adjusted for the loop 1 design.

2.3 Propeller Design

The isolated propeller was designed at Safran Tech using different fidelity levels, assessing aerodynamic performance and mechanical resistance [12]. The final propeller geometry featured 4 blades, the blade average chord c was equal to 0.18 m, while the blade radius R was equal to 1.65 m. The sense of rotation of all propellers was clockwise when viewed from the front of the rotor disk. The final propeller geometry was simulated along the mission points using RANS calculations on a sectorial mesh with the *elsA* CFD software (see part 3.2.2 for more detail). The propeller achieves the target thrust in cruise, equal to T = 1465 N, for a pitch value of $\theta_0 = 53.2°$, at a rotation velocity of 850 rpm. The blade section at r/R = 70% was used as a reference to define the blade pitch angle. The performance of the propeller along the mission is described in [12].

3 METHODS

Several aerodynamic tools, based on mid- and high-fidelity methodologies, have been applied in the assessment phase of the aerodynamics of the concept aircraft. A description of the main characteristics of these tools is briefly summarized in the present section.

3.1 Mid Fidelity Tools

3.1.1 RAMSYS

Two different codes have been used and compared to each other. CIRA used the RAMSYS solver [13], which is an unsteady, inviscid and incompressible free-wake vortex lattice Boundary Element Methodology (BEM) solver for multi-rotor, multi-body configurations developed at CIRA. It is based on Morino's boundary integral formulation for the solution of Laplace's equation for the velocity potential φ. The surface pressure distributions are evaluated by applying the unsteady version of Bernoulli equation, which is then integrated to provide the

forces and moments on the configuration. A computational acceleration was obtained by applying the parallel execution via the OpenMP API.

3.1.2 FlightStream

Safran Tech (ST) used the commercial software FlightStream [14] which is a viscous surface-vorticity solver able to deal with unstructured meshes. This allows to take into account complex geometries such as nacelles, fuselage and so on. Besides, boundary-layer development and its impact on performance is accounted for.

3.2 RANS

3.2.1 TAU

The numerical simulations based on the Reynolds-averaged Navier-Stokes (RANS) equations have been carried out with the *DLR TAU* code [15]. The turbulence effects were modeled with the Spalart-Allmaras formulation (SA) [16] with vortical and rotational flow correction based on the Spalart-Shur correction [17]. In order to model the propeller effects, an actuator disk approach based on 2D blade element momentum theory is implemented in *TAU*. Detailed information on the actuator disk implementation can be found in [18].

3.2.2 elsA

The RANS computations for the isolated propeller were performed using the *elsA* software [19]. A sectorial computational domain with periodic boundary conditions is used, the mesh is wall fitted on the blade geometry, with wall viscous boundary conditions. The modelling of turbulence was accounted for using the Kok k−ω turbulence model [20]. The k−ω model is chosen for its ability to accurately model close-wall phenomena. The Menter Shear Stress Transport (SST) correction is activated. The Reynolds numbers being in the order of 10^6 along the blade span and along the mission phases, the assumption is made that the computations can be carried out in fully turbulent mode, no transition model was implemented.

4 RESULTS

4.1 Comparison of Numerical Methods

Various numerical methods have been utilized within the aerodynamic studies. In order to classify the results, the methods were compared to each other on two test cases with the focus being on the modeling of propeller effects and its downstream effect the main wing under cruise flight conditions.

4.1.1 Isolated Propeller

The isolated propeller was computed under cruise flight conditions and the cruise flight design RPM. Figure 2 compares the propeller efficiency depending on the propeller thrust for the utilized numerical methods. The elsA results thereby represent RANS computations of an isolated Blade and can be viewed as a reference. All of the three methods, which consider viscous effects indicate a similar trend with the efficiency rising first towards the target thrust

and then decreasing again. The maximal deviation of the TAU and FlightStream (Viscous) computations with respect to the elsA results are 2.8 and 5.1 percentage points, respectively. Interestingly, the RAMSYS computations also show a similar trend with a higher maximal deviation of 6.5 percentage points. In contrast, the inviscid methods (elsA Euler and FlightStream) yield a rather linear decline in propeller efficiency for $T \geq 500$ N.

4.1.2 Installed Propeller

Safran Tech computed the loop 1.5 cruise flight configuration with varying degree of geometric complexity utilizing FlightStream with viscous effects. The results were then compared to the TAU results of the fully integrated loop 1.5 shape (full conf) including fuselage, wing, tail, nacelles, and propellers. The force and moment contributions from the tail were neglected in the comparison.

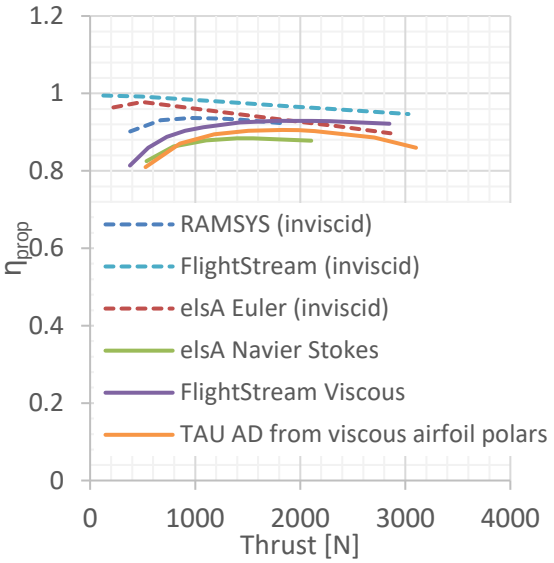

Figure 2: Efficiency of isolated propeller depending on thrust

The consideration of the main wing in the computations has a notable effect on the propellers' thrust and torque depending on the propeller id/position (Figure 3). Compared to the TAU computation, the trends of the thrust and torque distributions along the propellers agree well. Interestingly, the offset between the two methods increases if the nacelles are also considered in the geometry simulated with FlightStream. Moreover, TAU indicates a strong integration impact on the efficiency and a degradation of η_{prop} towards the wing tip. The integration impact and the variation along the span is estimated to be much less with FlightStream.

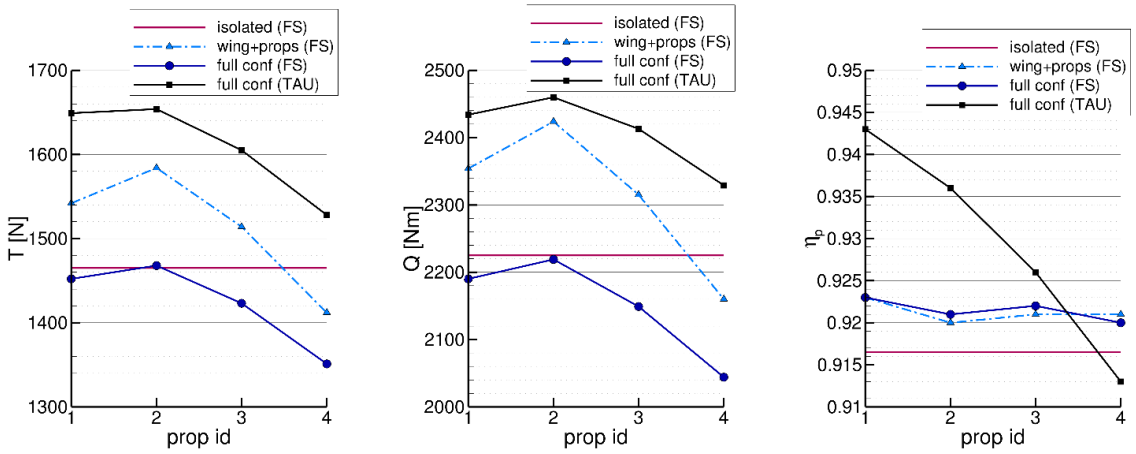

Figure 3: Installation effects on propeller metrics assessed with FlightStream and compared to fully installed case computed with TAU at α=0°

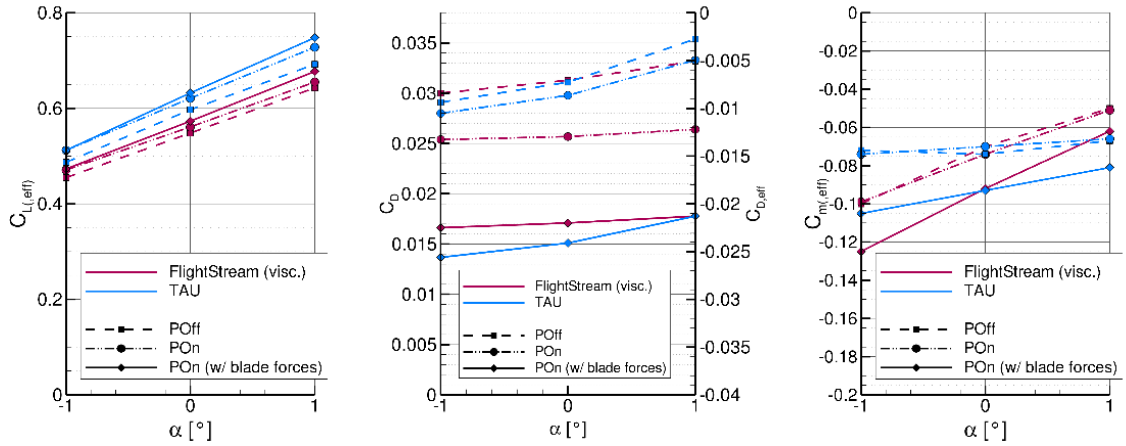

Figure 4: Comparison of lift (left), drag (center), and pitching moment (right) coefficients between FlightStream and TAU for power off (POff) and power on (Pon) conditions

Figure 4 compares the global coefficients of the fully integrated loop 1.5 geometry computed with FlightStream and TAU. Again, both methods indicate similar trends regarding the effect of the propeller effects and the angle of attack. FlightStream thereby yields a smaller impact of the propellers on the lift coefficient whereas the reduction in the drag coefficient due to the propellers' slipstream is notably stronger. The pitching moment at α=0° agrees well between the methods. The pitching moment gradient with respect to the angle of attack however is notably higher with FlightStream. The TAU results feature some small regions of flow separation that are not reflected in the FlightStream results an may explain the offsets to some extent.

4.2 Design Studies

4.2.1 Cruise Flight

Propellers' layout & position

This section illustrates the results of aerodynamic numerical simulations carried out on a configuration composed by a wing + an array of eight propellers installed in front of the wing leading edge. The main goal was the evaluation of the mutual influence between the wing and the array of propellers at three different locations of the array (propellers' layout: baseline, mid or close as shown in Figure 5) and at three different angles of attack.

Numerical setup

The geometric and cinematic symmetry conditions of the investigated test cases enabled the modelling of only one half of the configuration, the starboard side one, with a considerable saving of computational time. In CIRA setup the four propellers were all equal and four-bladed each. The hub was not modelled. In Safran Tech setup, the same blades were used for this wing/propeller layout and for the full aircraft configuration. The large diameter of the inboard nacelle hub required to cut the blade root to maintain a gap between the blades and the hub.

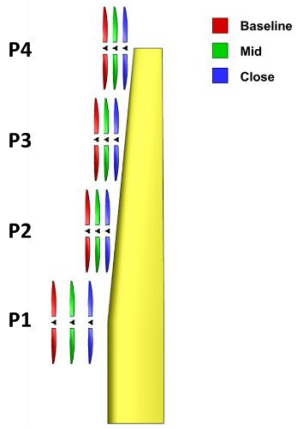

Figure 5: Spanwise positions of the propellers & the three different propellers' layouts

Results

a) Isolated propeller

An adjustment of the blade pitch angle θ_0 was necessary in order to obtain the nominal thrust T=1465 N of the single propeller in pure axial flight (AoA = 0°). Table 2 gives the adjusted pitch values to match the nominal thrust.

b) Installation effects

A comparison of the time-averaged rotor thrust and torque is shown in Figure 6 for the three layouts. The mutual effect between the wing and the propellers show a progressive increase in terms of thrust as the propellers approach the wing leading edge, so that the closer the propellers are to the wing the more thrust is produced. The wing presence tends to locally reduce the axial induced velocity at the propeller plane, thus increasing the effective blade pitch and consequently the thrust. Figure 6 shows that for the Baseline and Mid layouts, propeller P2 is the one that produces more thrust than the others. More discrepancies between CIRA and Safran results appear for the Close layout, for which Safran predicts significantly lower thrust for P2 and P3. As expected, the wing tip propeller P4 produces less thrust since wing loading gets lower towards the tip. Globally, the installed thrust predicted by Safran is lower than predicted by CIRA. The torque evaluated for the three layouts follows the same trend as the thrust, but for the Close layout the maximum torque is obtained for the innermost propeller P1. The increase in angle of attack leads to an increase in thrust but only negligible changes in the torque (not shown). Globally, the installed torque predicted by CIRA is lower than predicted by Safran.

Table 2: Blade pitch angle adjustment for nominal thrust

	Pitch (°)	T (N)	Q (N.m)
CIRA	53.81	1463	2228
ST: P1	51.26	1467	2222
ST: P2, P3,P4	51.11	1464	2228

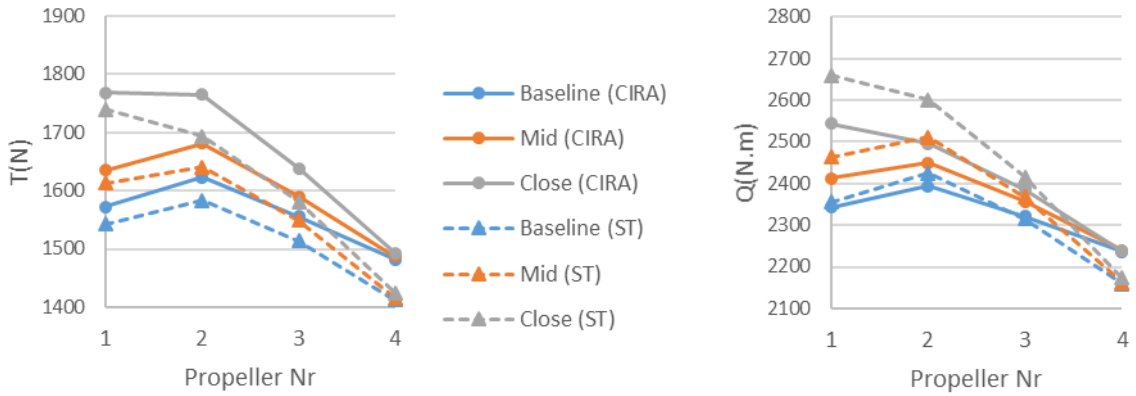

a) Thrust b) Torque

Figure 6: Installed propellers

Table 3 shows, for each propeller in axial flight (AoA = 0°), the thrust percentage increment for the Baseline, Mid and Close configurations with respect to the isolated propeller blade thrust.

Table 3: Thrust percentage increment of the three layouts with respect to the isolated propeller in axial flight (AoA = 0°)

	Baseline (%)		Mid (%)		Close (%)	
	CIRA	ST	CIRA	ST	CIRA	ST
P1	7.21	5.14	11.50	9.99	20.58	18.61
P2	10.68	8.18	14.68	12.07	20.37	15.69
P3	6.17	3.41	8.48	5.82	11.74	8.02
P4	1.12	-3.55	1.47	-3.32	1.85	-2.68

In order to rank the performances of the three layouts tested, the propulsive efficiency was evaluated from the calculated thrust and torque at the three angles of attack. The results, reported in Table 4, show that the efficiency progressively increases as the propellers approach the wing leading edge and also with angle-of-attack. However, Safran's results show a lower sensitivity to wing distance.

Table 4: Propulsive efficiency

	Baseline		Mid		Close	
AoA (°)	CIRA	ST	CIRA	ST	CIRA	ST
-1	0.942	0.917	0.947	0.917	0.963	0.915
0	0.945	0.918	0.953	0.917	0.974	0.916
1	0.953	0.923	0.965	0.923	0.991	0.922

A comparison of the computed rotor thrust and torque time histories, for the three layouts at AoA = 0°, is shown in Figure 7 and Figure 8, respectively. As the propellers approach the wing leading edge, the thrust and torque coefficients time histories show a progressive increase not only in their mean value but also in the amplitude of the oscillations, which can lead to an increase in vibratory loads and noise radiation.

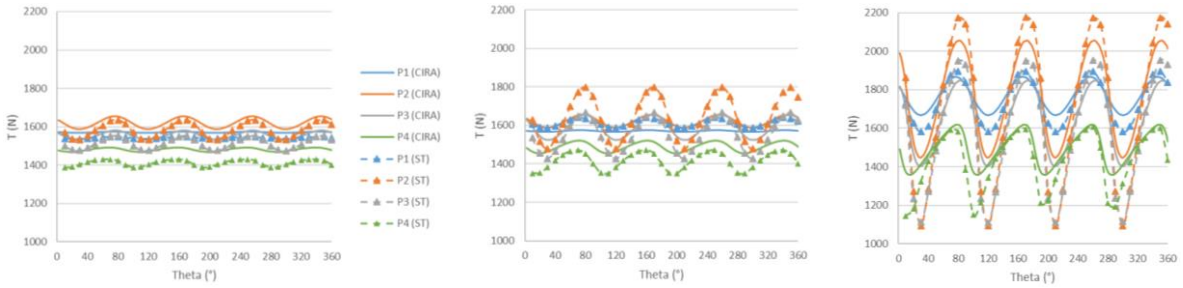

Figure 7: Propellers' thrust time history on one rotation. Baseline (left); Mid (centre); Close (right) – AoA = 0°

The installation effect of the propellers along the wing span of the aircraft produced changes in both lift and pitching moment of the configuration. A reference simulation was made for the isolated wing, without propellers, to evaluate its baseline lift and pitching moment. These values

were then compared, and reported in Table 5, with those referring to the configuration equipped with the propellers, at AoA = 0°, in the three different layouts. The propellers tend to slightly increase the wing lift and significantly reduce the (nose-down) pitching moment.

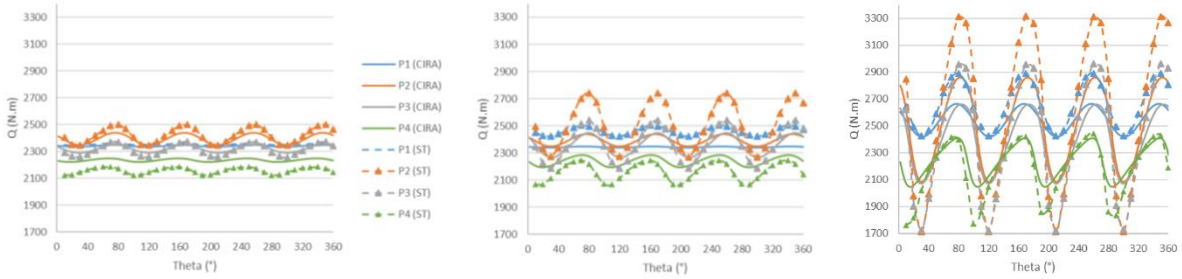

Figure 8: Propellers' torque time history on one rotation. Baseline (left); Mid (centre); Close (right) – AoA= 0°

Table 5: Force and moment coefficient comparison between the three different layouts (including blade forces) with respect to the isolated wing - AoA = 0°

AoA=0°	ΔCL vs isolated wing		ΔCmy vs isolated wing	
Layout	CIRA	ST	CIRA	ST
Baseline	2.42%	5.28%	-19.51%	-10.23%
Mid	2.28%	5.46%	-20.01%	-10.21%
Close	1.84%	5.65%	-20.51%	-10.00%

4.2.2 Low Speed

In order to assess the impact of the number of propellers and the propeller positions on the maximum effective lift coefficient under take-off conditions, 3D-RANS computations of the loop 0 take-off configuration have been carried out with TAU. In this study, the propulsor nacelles have been neglected. The parameters being varied were the streamwise position of the propellers with respect to the wing leading edge (ΔX), the vertical position of the propellers with respect to the wing leading edge (ΔZ), and the number of propellers (n).

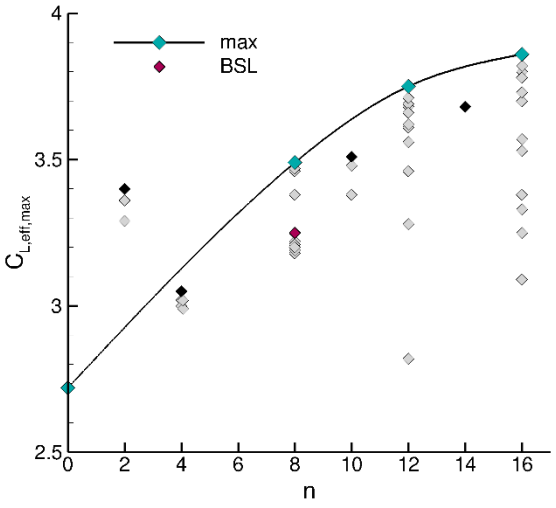

Figure 9: Maximum effective lift coefficient due to propeller slipstream effects depending on number of propellers

Figure 9 depicts the maximum effective lift coefficients (with forces acting on propeller blades) depending on the propeller count. The plot shows the results of all investigated cases with the black curve and the turquoise symbols representing the highest values achieved for each propeller count. The curves indicate a clear trend with the maximum effective lift coefficients increasing with rising propeller

count. However, the curves flatten towards higher n. With comparably high maximum effective lift coefficients, the cases with 2 propellers stand out. These cases do not utilize a wing tip propeller and thus the thrust is solely produced in a wing region of high base lift mainly caused by the large local chord length and flap deployment. As a result, the propeller blowing effect is comparably large. The figure also puts the $C_{L,eff,max}$ of the initial aircraft design (red symbol) into relation with the maximum lift augmentation potential.

It can be concluded that the maximum effective lift generally increases with the number of propellers. The effect, however, is highly dependent on the propeller positions. With 16 propellers $C_{L,eff,max}$ increases by as much as $\Delta C_{L,eff,max}$ = 1.14 (+42 %) for the present aircraft design due to slipstream deflection compared to $\Delta C_{L,eff,max}$ = 0.53 (+19 %) with the baseline 8 propeller design. However, this high value can only be achieved for low propeller positions that may have an adverse effect on the cruise flight performance. The dependency of $\Delta C_{L,eff,max}$ on the propeller position is less pronounced at large D_{prop}/c ratios, i.e. small numbers of propellers. Moreover, the increase in $C_{L,eff,max}$ appears to be limited due to the D_{prop}/c ratio becoming too small and unfeasible (vertical) propeller positions. Further details can be found in [5].

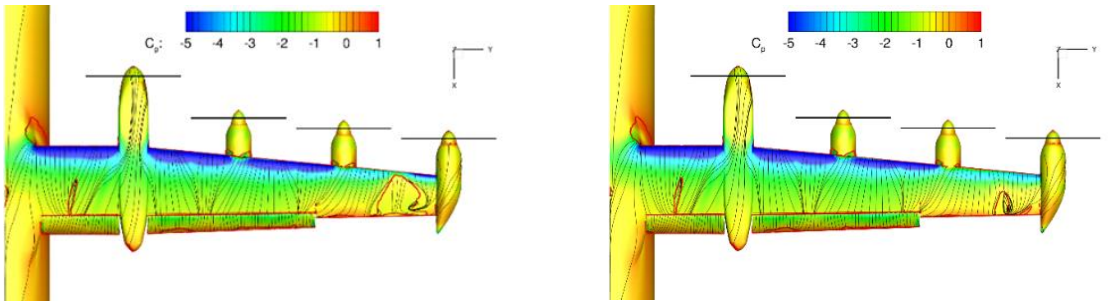

a) Baseline

b) Modified airfoil with leading edge droop and modified twist distribution

Figure 10: Surface pressure distribution, skin friction lines, and flow separation (c_f=0-iso-lines in red) of take-off configuration at maximum power, α=9°

Due to the highly loaded outboard wing in conjunction with the small taper ratio and the propeller slipstream effects, the high-lift configurations experience outboard flow separation even at low angles of attack. Therefore, the airfoil shape at the tip section was modified by means of 2D-RANS optimizations to increase the local α_{max} while maintaining high L/D values under cruise flight conditions. The final airfoil with leading edge droop increases α_{max} under low speed conditions by $\Delta\alpha_{max}$=3° while also increasing C_{L0}. The L/D ratio in cruise flight thereby remains comparable to the baseline airfoil at and around cruise flight conditions. The effect of the modified airfoil on the low speed performance on aircraft level was tested in conjunction with an additional adjustment of the twist distribution. In this case, the modifications showed a significant improvement (Figure 10). However, a preliminary lifting line assessment found an increase in the drag coefficient by ΔC_D=0.0007 due to the airfoil modification in conjunction with a modified twist angle.

Due to the utilization of slipstream deflection, the baseline high-lift design yields an excessive maximum effective lift coefficient in take-off configuration as shown in Figure 12[1].

[1] assuming that propeller effects can be considered for the determination of the reference stall speed

It was therefore investigated if the high-lift design can be modified to trade maximum effective lift for improved climb performance. Besides reducing the flap deflection, this was realized by re-designing the high-lift system with the flap gaps being sealed in take-off configuration (Figure 11). Using the target $C_{L,max}$ value for take-off ($C_{L,max,target}$=2.5) and the more conservative safety speed margin of 13% (the more conservative safety margin is used as the full utilization of slipstream deflection is considered), the minimum take-off safety speed is:

$$C_{L,V2min} = \frac{2.5}{1.13^2} = 1.96$$

The value represents the highest effective lift coefficient that would be flown during take-off under normal circumstances. After lift-off the aircraft accelerates further and the C_L will eventually decrease. Comparing the climb-ratio (Figure 13) of the baseline high-lift design with vented flaps and the one with sealed flaps, the latter yields higher values for $C_{L,eff} \leq 2.1$. While the difference is rather small at $C_{L,eff}$=1.96 it increases notably towards lower effective lift coefficients with the climb-ratio increasing by 12% at $C_{L,eff}$ = 1.37. Moreover, it is anticipated that the improvement in climb-ratio for $C_L \leq C_{L,V2min}$ can be further increased.

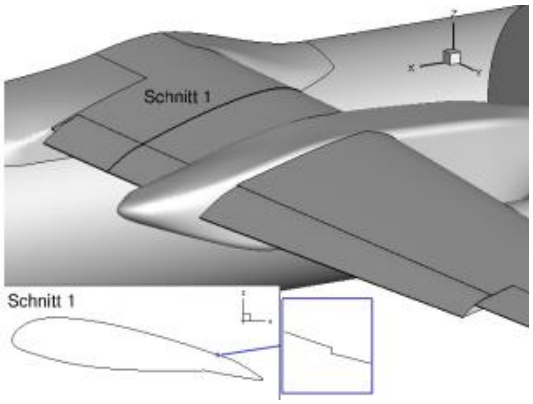

Figure 11: Overview of re-designed flap system with sealed flap in take-off configuration

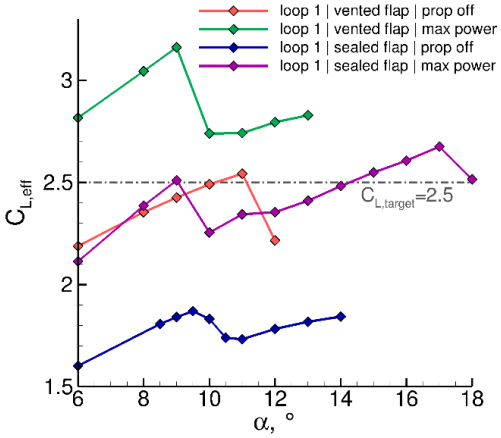

Figure 12: Effective lift coefficient depending on angle of attack

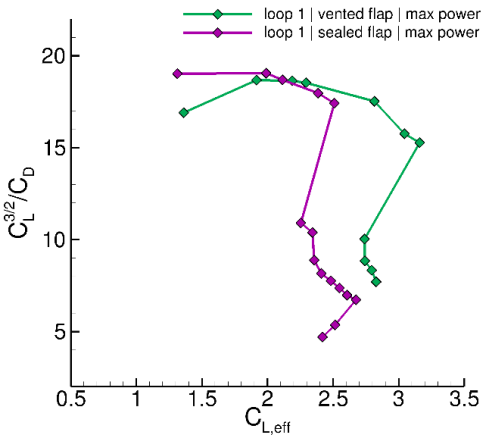

Figure 13: Climb ratio depending on effective lift coefficient

4.3 Performance Assessment

Design studies on the nacelle integration for the loop 1 status yielded an increase in aerodynamic performance of 10 % and a reduction in the required power of 6 % at mid cruise conditions [5]. The increase in the wing aspect ratio and the resulting reduction in the taper ratio made the integration of the rather large mid-/outboard nacelles (2 and 3) more challenging

(Figure 14). Without adapting the design, e.g. by increasing the taper ratio or moving the propellers further ahead of the wing, the pressure drag due to local flow separation will counter act the benefits of reduced induced drag. As a result, the lift-to-drag ratio of the loop 1.5 design increases at higher lift coefficients compared to the loop 1 design, whereas it decreases at low C_L values. At the loop 1 mid cruise design conditions, the L/D ratio for the full aircraft with untrimmed tail increases from 19.5 for loop 1 to 20.5 for loop 1.5.

The take-off configuration of the loop 1 design achieves a $C_{L,eff,max}$ of 2.54 with propellers off and 3.16 at maximum power. The landing configuration yields a $C_{L,max}$ of 2.64 with propellers off. More information on the high-lift performance can be found in [5].

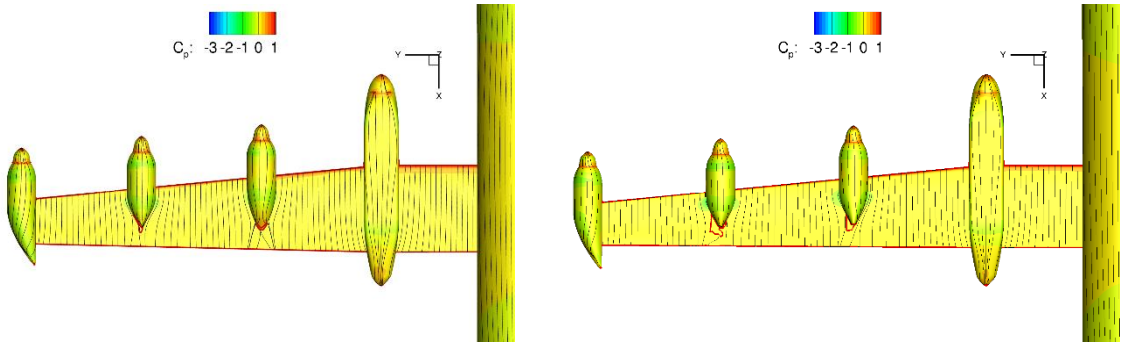

a) Loop 1 b) Loop 1.5

Figure 14: Surface pressure distribution and skin friction lines on the lower side of the wing at mid cruise conditions

5 CONCLUSIONS

The paper gives insight into the wide variety of numerical studies that were carried out on the aerodynamics of a propeller-driven regional aircraft with distributed electric propulsion within the IMOTHEP project. First, a comparison of the utilized methods is given. It shows generally good agreement between the viscous methods with regard to the trends of the isolated propeller efficiency while offsets exist between the codes with varying magnitude. For the installed case, the trends with regard to the influence of the main wing on the propellers in terms of thrust and torque generally agree between the mid-fidelity results from FlightStream and the RANS results from TAU. The impact on the propeller efficiency however is estimated to be substantially stronger by TAU than it is estimated by FlightStream. Nevertheless, the utilized mid fidelity methods represent an efficient way to analyze transient effects such as propeller load oscillations. Assessing the impact of the propeller distance to the wing, RAMSYS and FlightStream indicate a notable increase in magnitude of propeller thrust and torque oscillations if the propellers are positioned closer towards the leading edge. While the propeller efficiency is thereby projected to increase, the effective lift and pitching moment coefficients are estimated to be rather unaffected. A study on the number of propellers and streamwise propeller position with regards to lift augmentation capabilities in take-off found a maximum increase in the maximum effective lift coefficient of 1.14 (+42%) when utilized 16 propellers. This compares to a $\Delta C_{L,eff,max}$ increase of 0.53 (+19%) for the baseline design. If the lift augmentation capabilities in take-off cannot be utilized because of insufficient maximum lift capabilities in

approach/landing, it may be possible to exploit the lift augmentation capabilities in take-off by improving the aerodynamic efficiency during climb as the study indicates.

High loadings at the outboard wing amplified by propeller slipstream effects cause premature flow separation in this region in high-lift configurations. An initial attempt to locally modify the airfoil by adding leading edge droop indicated that the outboard flow separation could be removed at the cost of a drag penalty under cruise flight conditions.

The detailed integration design indicates that nacelles of DP concepts can have a meaningful impact on the cruise flight as well as low speed performance due to their size and position. The studies on the present aircraft concept indicate that either the taper ratio of the wing has to be increased or the nacelle ahead of the aileron has to be be moved towards the front in order to reduce adverse nacelle integration effects under cruise flight conditions. With regards to the low speed performance, nacelle strakes were found to have the potential to mitigate the adverse effects of the nacelles as shown in [5].

The integration design yielded an increase in aerodynamic performance of 10 % and a reduction in the required power of 6 % compared to the baseline shape resulting in a L/D ratio for the full aircraft with untrimmed tail of 19.5 (loop 1) under mid cruise conditions.

ACKNOWLEDGMENTS

This project has received funding from the European Union’s Horizon 2020 research and innovation program under grant agreement No. 875006 IMOTHEP.

REFERENCES

[1] S. Biser, G. Atanasov, M. Hepperle, M. Filipenko, D. Keller, D. Vechtel, M. Boll, N. Kastner and M. Noe, "Design Space Exploration Study and Optimization of a Distributed Turbo-Electric Propulsion System for a Regional Passenger Aircraft," in *Proc. AIAA Propulsion and Energy 2020 Forum*, 2020.

[2] D. Keller, "Towards higher aerodynamic efficiency of propeller-driven aircraft with distributed propulsion," *CEAS Aeronautical Journal*, vol. 12, no. 4, 2021.

[3] M. Schollenberger, B. Kirsch, T. Lutz, E. Krämer and J. Friedrichs, "Aerodynamic interactions between distributed propellers and the wing of an electric commuter aircraft at cruise conditions," vol. 15, no. 5, 2024.

[4] S. Y. Yoo, J. C. Duensing, K. A. Deere, J. K. Viken and M. Frederick, "Computational Analysis on the Effects of High-lift Propellers and Wing-tip Cruise Propellers on X-57," in *Proc. AIAA AVIATION 2023 Forum*, 2023.

[5] D. Keller, "Aerodynamic Investigation of the High-Lift Performance of a Propeller-Driven Regional Transport Aircraft with Distributed Propulsion," *Journal of Physics: Conference Series*, vol. 2526, no. 1, p. 012007, 2023.

[6] M. F. Beckers, M. Schollenberger, T. Lutz, D. Bongen, R. Radespiel, J. L. Florenciano and E. Funes-Sebastian, "CFD investigation of high-lift propeller positions for a distributed propulsion system," in *Proc. AIAA AVIATION 2022 Forum*, 2022.

[7] T. K. Lindner, P. Scholz, J. Oldeweme and J. Friedrichs, "Experimental propeller placement analysis for a distributed propulsion wing section in high lift configuration," in *Proc. AIAA AVIATION 2023 Forum*, 2023.

[8] A. Gothow, A. Bardenhagen, J. Weiss, D. P. Bergmann, J. Denzel and A. Strohmayer, "Experimental Parameter Study of Distributed Electric Propulsion on a 2D Wing Model in High-Lift Configuration," in *Proc. AIAA AVIATION 2023 Forum*, 2023.

[9] L. G. Stoica, A. Di Marco, R. Camussi, E. De Paola, U. Iemma, L. Burghignoli, G. Palma, N. Paletta, N. Pepelas, J. Beretta, A. Visingardi, A. Pagano, G. Mingione, C. Izzo, G. Andreutti, M. Barbarino, D. Quagliarella, P. Vitagliano, R. Pasta, L. Flamini and F. Rusconi, "VENUS Project: Investigation of Distributed Propulsion Noise and its Mitigation Through Wind Tunnel Experiments and Numerical Simulations," in *Forum Acusticum* , Turin, Italy, 2023.

[10] A. Visingardi, M. Barbarino and D. Quagliarella, "and Acoustic Design Optimization of a Multiple Propeller Combination for Distributed Electrical Propulsion," in *15th World Congress on Computational Mechanics (WCCM-XV), 8th Asian Pacific Congress on Computational Mechanics (APCOM-VIII) Virtual Congress*, 2022.

[11] G. Atanasov, "Plug-In Hybrid-Electric Regional Aircraft Concept for IMOTHEP," in *12th EASN International Conference on Innovation in Aviation and Space for opening New Horizons*, Barcelona, Spain, 2022.

[12] Y. Maldonado, F. Tong-Yette, L. Delcambre and B. Rodriguez, "Propeller predesign for distributed propulsion architectures," in *3AF - Towards Sustainable Aviation Summit*, Toulouse, 2022.

[13] A. Visingardi, A. D'Alascio, A. Pagano and P. Renzoni, "Validation of CIRA's Rotorcraft Aerodynamic Modelling System with DNW Experimental Data," in *22nd European Rotorcraft Forum*, Bristol, UK, 1996.

[14] V. Ahuja and R. J. Hartfield, "Aerodynamic Loads over Arbitrary Bodies by Method of Integrated Circulation," *Journal of Aircraft*, vol. 53, no. 6, p. 1719–1730, 2016.

[15] T. Gerhold, "Overview of the Hybrid RANS Code TAU," *MEGAFLOW -- Numerical Flow Simulation for Aircraft Design, Notes on Numerical Fluid Mechanics and Multidisciplinary Design*, vol. 89, pp. 81-92, 2005.

[16] P. R. Spalart and S. R. Allmaras, "A one-equation turbulence model for aerodynamic flows," in *30th Aerospace Sciences Meeting and Exhibit*, 1992.

[17] M. L. Shur, M. K. Strelets and P. R. Spalart, "Turbulence Modeling in Rotating and Curved Channels: Assessing the Spalart-Shur Correction," *AIAA Journal*, vol. 38, no. 5, pp. 784-792, 2000.

[18] A. Raichle, "Flux Conservative Discretization of the Actuator Disk Model as a Discontinuity Surface," Ph.D. Thesis, Technical University Braunschweig, Braunschweig, Germany, 2017.

[19] L. Cambier, S. Heib and S. Plot, "The Onera elsA CFD software : input from research and feedback," *Mechanics Industry, EDP Sciences*, vol. 14, no. 3, pp. 159-174, 2013.

[20] J. Kok, "Resolving the dependence on freestream values for the k-omega turbulence model.," *AIAA Journal*, vol. 38, no. 7, pp. 1292-1295, 2000.